Arabian Journal of Chemistry 16 (2023) 105311

Contents lists available at ScienceDirect

Arabian Journal of Chemistry

journal homepage: www.sciencedirect.com

Original article

On the optimal Cs/Co ratio responsible for the N_2O decomposition activity of the foam supported cobalt oxide catalysts

Anna Klegova [a], Kateřina Pacultová [a,*], Tomáš Kiška [a,b], Joanna Gryboś [c], Zbigniew Sojka [c], Lucie Obalová [a]

[a] Institute of Environmental Technology, CEET, VSB-Technical University of Ostrava, 17. listopadu 15/2172, Ostrava 708 00, Czech Republic
[b] Faculty of Materials Science and Technology, VSB-Technical University of Ostrava, 17. listopadu 15/2172, Ostrava 708 00, Czech Republic
[c] Faculty of Chemistry, Jagiellonian University, Gronostajowa 2, 30-387 Kraków, Poland

ARTICLE INFO

Article history:
Received 14 March 2023
Accepted 24 September 2023
Available online 27 September 2023

Keywords:
Cobalt oxide
Ceramic foam
Supported Catalyst
N_2O decomposition
Cesium effect

ABSTRACT

Structured foam catalysts for N_2O decomposition containing Co and Cs were prepared via conventional and organic-assisted impregnation method (acetic acid, citric acid, glycerol, glycine, urea). Organic-assisted impregnation caused higher abundance of smaller particles and different faceting. Glycerol usage leads to increase of specific rate constant for N_2O decomposition, urea leads to its decrease. The optimal amount of Cs in Co_3O_4 deposited on the foam was 2–3 times higher than in the bulk Co_3O_4-Cs due to the dispersion of part of the Cs species over the bare support. The use of glycerol caused a better surface coverage by spinel phase, thus leaving less space for spreading the cesium on the support instead of on the spinel phase. The positive effect of glycerol on the performance of the catalysts with optimized cesium content was attributed to refaceting of the spinal nanocrystals, and greater resistance of the (100) planes to gaseous NO/H_2O contaminates.

1. Introduction

N_2O emissions represent the most significant anthropogenic contribution to ozone-depleting substance emissions and the third most significant contribution to greenhouse gas emissions (Ravishankara et al., 2009). N_2O emission control can be applied most easily to large point sources of direct N_2O emissions from industry and energetics, such as nitric acid production (Frutos, 2018; Pérez-Ramírez et al., 2003) although methods for decreasing N_2O concentration in ambient air have been also studied (Reli et al., 2019; Kočí et al., 2019). One of the possibilities for N_2O emission abatement is treatment of tail gases by direct catalytic decomposition (European Commission, 2007). Oxidic catalysts based on group VIII transition metals (Rh, Ir, Co, Fe, Ni) exhibit high catalytic activities in this reaction. Spinel-type oxides containing Co (e.g. $MgCo_2O_4$, $ZnCo_2O_4$, Co_3O_4) (Kapteijn et al., 1996; Konsolakis, 2015; Russo, 2007) are especially promising. Significant improvement in Co_3O_4 catalytic activity is observed with the addition of an alkali metal promoter (Cs, K) (Wójcik et al., 2020).

Although Co_3O_4-Cs catalysts possess high deN_2O activity, it is difficult to shape them into pellets. Furthermore, in bulk-shaped catalysts, the relatively pricey active components would not be utilized efficiently (Obalová et al., 2019). Supported catalysts offer various advantages for industrial applications: dispersion of the active components on a large geometric surface of the support, mechanical properties and stability, lower pressure drop, as well as better mass and heat transfer in the catalyst (Meille, 2006; Richardson et al., 2003; Richardson et al., 2000; Twigg and Richardson, 2002). The deposition procedure for the potassium or cesium modified $Co_3O_4|\alpha\text{-}Al_2O_3|$cordierite structured catalyst for low temperature N_2O decomposition was optimized by the Kotarba group (Wójcik et al., 2018; Grzybek et al., 2017; Wójcik et al., 2018). Our group studied the use of commercially available open cell foam as a support for the N_2O decomposition catalyst with respect to the deposition procedure and active phase composition (Klegova et al., 2019), foam material composition (Pacultová et al., 2020), foam cell size, washcoat influence (Klegova et al., 2022) and loading (Klegova et al., 2023).

Conventional wet impregnation is the simplest way to obtain Co_3O_4 catalyst on ceramic foam, however impregnation using a suitable organic agent may lead to improved catalyst activity and other properties (Grzybek et al., 2017; Gudyka et al., 2017; Shi et al., 2012). Organic assisted impregnation combines in one step impregnation and solution combustion approaches (Deganello and Tyagi, 2018; Specchia et al.) and can be found in the literature under different names, such as surface impregnation combustion (González-Cortés and Imbert, 2013). The organic agent has a dou-

* Corresponding author.
E-mail address: katerina.pacultova@vsb.cz (K. Pacultová).

https://doi.org/10.1016/j.arabjc.2023.105311
1878-5352/

ble function, being the metal ions complexant, thus facilitating homogeneous mixing of the cations in solution and preventing selective precipitation of the metal ions during water removal, as well as fuel (Varma et al., 2016). The process is complex and often consists not only of the decomposition of the metal precursor and the combustion of the fuel but also complexation and redox reactions between the fuel and the metal precursor, and also reactions between the decomposition products (Zavyalova et al., 2009; Novitskaya et al., 2021).

The solution combustion synthesis/organic assisted impregnation for the preparation of Co_3O_4-based catalysts on various supports for redox reactions, including N_2O decomposition, has been reported in (Grzybek et al., 2017; Gudyka et al., 2017; Zavyalova et al., 2007; Wyrwalski and e. al, , 2007; Ciura et al., 2017; Russo et al., 2007; Bera, 2019). Compared to the catalyst prepared by conventional impregnation, these exhibited a smaller crystallite size, a larger specific surface area, better reducibility and dispersion attributed to the combustion behavior of cobalt precursors and fuels (Zavyalova et al., 2007; Wyrwalski and e. al, , 2007). For the Co_3O_4/Al_2O_3 catalysts for N_2O decomposition, it was shown that the preparation method influenced the phase composition, morphology, radial active phase distribution and particle size distribution of the resulting catalysts, while the most active catalysts were those prepared by organic-assisted methods, with favorable phase composition and dispersion (Grzybek et al., 2017). The effect of varying content of glycerol used for preparation of Co_3O_4 on α-Al_2O_3 extrudates was shown in (Gudyka et al., 2017) where higher glycerol content lead to higher deN_2O catalyst activity linked with beneficial changes in the nanoscale morphology and dispersion of the active phase. Yoshino even synthesized a potassium-modified Co_3O_4 powder catalyst using glycine as a fuel (Yoshino et al., 2011). The optimization of cesium and potassium promoter loading on $Zn_{0.4}Co_{2.6}O_4/\alpha$-$Al_2O_3$ catalysts for N_2O abatement prepared by incipient wetness impregnation of powder support with 30 vol% glycerol-aqueous solution of cobalt and zinc nitrates showed that optimal loading is in a rather narrow range (0.5–3 atoms/nm^2), and specific for each individual catalytic system (Ciura et al., 2017).

However, there is no study on the use of combustion-based methods for the preparation of catalyst for N_2O decomposition deposited on the ceramic foam support. Our previous findings on the use of ceramic foam-supported cobalt oxide catalysts showed that one of the most important parameters is the optimal Cs/Co ratio (Klegova et al., 2022; Pacultová et al., 2020), which often depends on a different level of cobalt oxide aggregation and different level of cesium dispersion. Since generally using organic agents during catalyst preparation affects microstructure of the catalyst and dispersion of the individual active components, this is a key area to be explored furthermore.

In the present work, the preparation of active Cs-Co_3O_4-open cell ceramic foam deN_2O catalyst is addressed, aiming to optimize the preparation procedure by using organic-assisted impregnation method and finding the optimal cesium loading. The operative parameters were (i) different organic impregnation agents (acetic acid, citric acid, glycerol, glycine, urea) acting as fuels while keeping constant cobalt to fuel molar ratio, resulting in different fuel rich or lean conditions (ii) Cs-promoter loading on the Co_3O_4 active phase (0–4 wt%) deposited by conventional and glycerol-assisted impregnation. For the most active supported catalysts, the activity was assessed in process stream conditions containing in addition to N_2O also O_2, H_2O and NO_x. Different characterization techniques were used to explain the observed differences in the catalytic activity, and connect the results with the morphology and localization of the catalytically active components in/on the foam support in relation to preparation process used.

2. Experimental methods

2.1. Catalyst preparation

Several sets of catalysts differing in the composition of the active phase and deposition procedure were prepared in order to study effect of:

1) various organic impregnation agents,

2) glycerol concentration in impregnation solution,

3) cesium loading for organic free synthesis in bulk and supported catalysts,

4) cesium loading for glycerol assisted deposition in supported catalysts.

The effects 1) and 2) were elucidated on catalyst non-modified by cesium.

The first series of catalysts was prepared using different organic impregnation agents: acetic acid (Ace), citric acid (Cit), glycerol (Glr), glycine (Gly), and urea (Ure). Solutions were prepared by dissolving $Co(NO)_3{\cdot}6H_2O$ and an organic agent in water and diluting the solution to the desired concentration (Table S1). Compared to the rest of the series, a lower solution concentration was used to accommodate the preparation conditions for different solubility of each organic agent. The molar ratio of the organic agent to Co^{2+} ion in the solutions was always 1:1. A catalyst prepared by conventional (organic-free) impregnation (*c.i.*) was prepared as well. The catalysts are labeled as the active phase low-content series *L* using a three-letter abbreviation of the organic agent used, e.g. *L(Ace)*.

The second series of catalysts was prepared using glycerol as an impregnation agent with a 2:1 and 1:1 glycerol to Co^{2+} ion molar ratio. Solutions were prepared by mixing an appropriate amount of glycerol with water to volume and subsequently dissolving $Co(NO_3)_2{\cdot}6H_2O$ at a higher concentration of Co^{2+} compared to the *L* series (Table S1). The catalysts are labeled as the high-content series *H* using the numerator part of the glycerol to Co molar ratio, e.g. *H(Glr2)*. A catalyst prepared by conventional (organic-free) impregnation (*c.i.*) was also prepared for comparison.

The third series was prepared by conventional impregnation with the molar ratio of Cs^+ to Co^{2+} ions in the solution 1:150, 2:150, 3:150, 4:150, 5:150, 6:150 nominally resulting in the wt.% of Cs in the active phase being 1, 2, 3, 4, 5, 6, respectively. Solutions were prepared by dissolving weights of $Co(NO_3)_2{\cdot}6H_2O$ and $CsNO_3$ in a volume of water (Table S1). The catalysts are labeled as *c.i.* using Cs and nominal wt.% of Cs in the active phase, e.g. *c.i.(Cs2)*. To see the effect of the amount of cesium for the supported and also unsupported catalyst, the bulk active phase in a powder form was prepared from the parent nitrate solutions by drying at 105 °C and subsequent calcination for 4 h at 500 °C. The samples were labelled as *bulk* and Cs appended by nominal wt.% of Cs in active phase, e.g. *bulk*(Cs2).

The fourth series consists of Cs-doped catalysts prepared by glycerol-assisted impregnation with glycerol to Co^{2+} ion molar ratio in the solution 1:1 and Cs^+ to Co^{2+} ion molar ratio equal to those used for the third series i.e. 1:150, 2:150, 3:150, 4:150, 5:150, 6:150. The solutions were prepared by mixing appropriate amount of glycerol with water to volume and subsequently dissolving weights of $Co(NO_3)_2{\cdot}6H_2O$ and $CsNO_3$ (Table S1). The catalysts are labeled as *Glr* series using Cs and nominal wt.% of Cs in active phase, e.g. *Glr(Cs2)*.

For all catalysts commercially available ceramic foam (LANIK, Vukopor A; manufacturer declared composition: 85 wt% Al_2O_3, 14 wt% SiO_2, 1 wt% MgO, 10 ppi porosity) the support in the form of cylinder (48 mm diameter, 20 mm height) was first cleaned with ethanol and dried in air at 105 °C to constant weight. The foam was then immersed in an impregnation solution heated to 60 °C for

20 min. After the foam was removed from the solution, the excess solution was left to escape freely. The foam was then dried in air at 105 °C for 4 h and calcined in air at 500 °C for 2 h with a heating rate of 4 °C min^{-1}.

2.2. Catalyst characterization

Atomic absorption spectroscopy (AAS) was used to determine the chemical composition of the active phase. X-ray diffraction analysis (XRD) was used to characterize the catalyst crystallographic properties and phase composition. N_2 physisorption (S_{BET}) was used to characterize the catalyst surface area. Scanning electron microscopy (SEM) was used to investigate the catalyst morphology. Temperature programmed reduction by H_2 (H_2-TPR) was used to characterize the catalyst reducibility. For N_2 physisorption, H_2-TPR and XRD analyses, the samples were prepared by crushing the catalysts and grinding them in Pulverisette 6 (Fritsch) planetary mill using a zirconia grinding mill and balls and sieving to obtain particles of size below 165 μm. Information on ceramic foam support can be found in (Pacultová et al., 2020).

The chemical composition was determined by AAS using Analytik Jena ContrAA 700 spectrometer after dissolving the samples in aqua regia by heating them to 200 °C in a microwave reactor Ethos UP (Milestone, IT).

Nitrogen physisorption at − 196 °C was performed on 3Flex automated volumetric apparatus (Micromeritics Instruments, USA) after degassing the material (fraction < 0.25 mm) at 150 °C for more than 24 h under vacuum below 1 torr. Specific surface area was evaluated by the BET method.

Scanning electron microscope Quanta FEG 450 (FEI) with EDS microprobe analysis APOLLO X (EDAX) was used for the characterization of the catalyst morphology. The images were taken using secondary electron and backscattered electron detectors at 15 kV. Microprobe analysis was performed with the EDAX detector and processed with the EDAX software.

Temperature-programmed reduction by hydrogen (TPR-H_2) was carried out on AutoChem II 2920 equipment (Micromeritics, USA). Prior to the TPR experiments, the samples (fraction < 0.2 m m) were outgassed in the flow of pure helium (50 ml min^{-1}) at 500 °C for 60 min. Then, the TPR runs were performed in the flow of 10 mol. % H_2/Ar (50 ml min^{-1}) in the temperature range 20 – 995 °C or 20–450 °C (for Cs modified samples) with the heating rate of 20 °C min^{-1} and isothermal step at 450 °C for the next 40 min. Water vapor formed during TPR was captured in a cold trap.

SmartLab X-ray powder diffractometer (Rigaku, Japan) equipped with D/teX Ultra 250 position sensitive detector and Co tube (CoKα, λ_1 = 0.178892 nm, λ_2 = 0.179278 nm) was used for phase composition and microstructural determination of prepared catalysts. Recorded patterns were evaluated with appropriate software and compared to ICDD database (PDF-2). Coherent domain size of spinels l_D was calculated from the broadening of the diffraction peak (3 1 1) using Scherer equation $l_D = 0.9 \cdot \lambda / \beta \cdot \cos\theta$, where λ is wavelength of the used radiation, β is diffraction width and θ is diffraction position (in 2θ scale).

Particle size analysis and morphology of the cesium-doped spinel nanocrystals adhered to the support were studied using a FEI Tecnai Osiris transmission electron microscope equipped with an X-FEG Schottky field emitter operating at the voltage of 200 kV. Information about the spatial distribution of the elements in the samples was obtained by EDX analysis, using a windowless detector (Super-X EDX) and the Bruker Esprit software. Prior to the observations, the samples were placed on a copper grid covered with a holey carbon film. For detailed shape analysis of spinel nanocrystals, scanning transmission electron microscopy (STEM) measurements were carried out. Z-contrast imaging was performed using a high-angle annular dark-field detector (HAADF), and the camera length was kept in the range 330–550 mm to maximize the signal intensity. Cobalt spinel particle size analysis was performed using DigitalMicrograph (Gatan) software (Digital Micrograph, 2007). The nanocrystal shape retrieving was based on gradient analysis of the recorded HAADF STEM images. The procedure is based on the Z-contrast analysis using calibrated HAADF STEM images and involves quantification of the relation between the HAADF STEM image intensity (the grey value) and the thickness of the specimen, followed by image gradient analysis to retrieve the diagnostic features of the shape (the diagnostic edge pattern exhibited by the nanocrystals). The analysis was performed employing the Canny algorithm (Canny, 1986) implemented in FeatureJ (FeatureJ, 2003) software as part of the ImageJ package for image processing (Rasband, 1997). The determined edge pattern provided the local orientation of the observed nanocrystals and was used for assigning the (x; y) coordinates of the identified vertices in the observed two-dimensional images. Completed by default values of the missing z coordinates, they were used as input for the convex hull algorithm to obtain the tentative polyhedral shape of the nanocrystal, considering constraints imposed by the spinel crystal symmetry. A more detail description of this method can be found elsewhere (Gryboś et al., 2021). The imaging conditions were adjusted in such a way that the image contrast originates mainly from the changes in the thickness of the examined nanocrystals. By combining the information on the spinel structure with the information on the retrieved edge pattern and the variation of the sample thickness, it was possible to determine the shape of the examined spinel nanocrystals using the reversed Wulff construction (Wulff, 1901).

2.3. Catalyst testing

The catalyst in the form of cylinder (48 mm in diameter, 20 mm in height) was loaded into a fixed-bed reactor (50 mm inner diameter) filled with inert ceramic rings. Before testing, the catalyst was heated to 450 °C at a rate of 6 °C min^{-1} and kept at 450 °C for 1 h under N_2 flow. Reaction steady state was evaluated for temperatures in the range of 300–450 °C with temperature step of 30 °C. The N_2O concentration of the outlet mixture was continuously measured using the GMS810 (Sick) infrared N_2O analyzer. The composition of the inlet mixture was set to 0.1 mol.% N_2O in N_2 and determined at the beginning and at the end of each catalytic test. Tests were carried out under atmospheric pressure. For the low spinel content catalysts, GHSV = 1080 $(m^3\ h^{-1})_{gas}(m^3)_{cat.bed}$ was used; with sample sizes in the range 33.3–33.6 ml, corresponding to the volume flow rates of 599–605 ml min^{-1}. For the high spinel content catalysts, GHSV = 1500 $(m^3\ h^{-1})_{gas}\ (m^3)_{cat.bed}$ was used; with sample sizes 33.3–33.7 ml corresponding to the volume flow rates of 833–843 ml min^{-1}. Selected samples were also tested in simulated nitric acid plant tail gas at three different inlet gas compositions (0.1 mol.% N_2O, 0–5 mol.% O_2, 0–2 mol. % H_2O, 0–0.02 mol.% NO, balance N_2) at GHSV = 1500 $(m^3\ h^{-1})_{gas}(m^3)_{cat.bed}$. The effect of external diffusion was previously tested for catalysts deposited on ceramic foams with a pore density of 10 ppi; effect of external diffusion was confirmed to be insignificant at volume flow rates exceeding 585 ml min^{-1}.

Testing of the bulk Co_3O_4-Cs (particle size of 0.160–0.315 mm) was performed in the reactor with diameter of 5.5 mm at total flow rate of 100 ml min^{-1} (21 °C, 101325 Pa) and GHSV = 60 L $g^{-1}h^{-1}$. The catalysts were activated at 450 °C for 1 h in an inert gas, then the N_2O catalytic decomposition at 450 °C was measured for 10 h. After this period, where stable performance was verified, the temperature dependence of conversion was launched with cooling rate of 5 °C min^{-1} and the catalysts activity was measured for 2 h at

each temperature (450–330 °C). The N_2O conversion was calculated from the data obtained at steady state.

3. Results and discussion

3.1. Effect of organic impregnation agents

The preparation method is based on a fast-redox reaction between a fuel and an oxidant in the presence of metal cations. Organic impregnation agents act as fuel during catalyst preparation, while metal precursors themselves are oxidants. The role of organic agent is to interact with metal cations by chelating and creating a network to maintain the metal cations homogeneously fixed in their positions during combustion and to establish a good connection between the fuel and the oxidant moieties. During combustion, the fuel is oxidized by the oxidants, while metal cations take oxygen from the oxidants and convert into the corresponding oxides (Deganello and Tyagi, 2018). Combustion conditions generally depend on the chemical nature of the reactive solution formed; therefore, on the type of fuel and the ratio of fuel to oxidizer (Varma et al., 2016).

In our case, we decided to test different fuel types, specifically acetic acid and citric acid representing fuels with carboxylic groups, glycerol as a fuel containing the hydroxyl groups, glycine combining the carboxylic and amino groups, and urea containing the amino functions. These categories should have different complexing abilities, and the intensity of the combustion reaction should differ. Furthermore, we used solutions with a constant molar ratio of cobalt and organic agent (1:1) resulting in different fuel rich (glycerol φ = 1.4, citric acid φ = 1.8) or lean (acetic acid φ = 0.8, glycine φ = 0.9, urea φ = 0.6) conditions, defined based on calculations of the propellant chemistry (Deganello and Tyagi, 2018). The glycerol effect was also tested for the sample with two different Co_3O_4 loadings and for two different molar ratios of cobalt to glycerol in solution being 1:1 and 1:2, respectively. The 1:2 ratio was chosen on the basis of the general recommendation for reasonable fuel amount to be equal to twice the total molar amount of metal cations according to (Deganello and Tyagi, 2018; Deganello, 2017).

3.2. Catalyst preparation and characterization

Table 1 shows the physicochemical properties of the prepared catalysts: weight content of the active phase ($w_{Co_3O_4}$), crystallite size (l_D) and lattice parameter (a) of the active phase, BET specific surface of the catalyst (S_{BET}) and calculated specific surface of the active phase $S_{Co_3O_4}$. Properties of the ceramic foam substrate, as well as those of the catalyst prepared by conventional impregnation under the same conditions (but for the catalyst containing Cs-Co_3O_4 active phase) as those used for the *H(c.i.)* sample here, can be found elsewhere (Pacultová et al., 2020).

The weight content of the active phase was determined as the weight difference between the cleaned and dried foam prior to the impregnation and the catalyst after calcination. The values found for high-content catalysts agree with previous research (Pacultová et al., 2020), where conventional impregnation under the same conditions led to an active phase content of 5.4 wt%. As expected, the amount of active components deposited on the low-content catalysts (prepared from an impregnation solution with a lower concentration of cobalt nitrate concentration) is lower, being approximately 3.2 wt%.

XRD diffractograms of the prepared catalysts are shown in Fig. 1. In all the prepared catalysts, a phase corresponding to cobalt spinel oxide (ICDD PDF-2 00–042-1467) was detected along with corundum (Al_2O_3) (01–075-1862) and mullite ($Al_{4.54}Si_{1.46}O_{9.73}$) (01–079-1456) phases present in the foam support (for details see Table S2). The unmarked low-intensity lines (38,5°) may be attributed to the K β lines of the used X-ray source. Due to the low content of the Co_3O_4 active phase, the high intensity of support diffraction peaks complicates the evaluation of the structural parameters of the active phase.

The mean size of the crystallites was calculated according to the Scherrer equation from full width at half maximum (FWHM) of the spinel (311) line, corrected for the instrument resolution (LaB_6) (Table 1). In the low-content catalysts, conventional impregnation leads to crystallite size 60 nm, while organic-assisted impregnation regardless of the organic agent leads to approximately half values around 32 nm with the exception of *L(Ace)* sample having *Lc* only slightly lower (51 nm). In high spinel content catalysts, conventional impregnation results in crystallite size of 148 nm, glycerol-assisted impregnation at the 1:1 glycerol to cobalt molar ratio halves this value to 81 nm, and doubling of the glycerol content to 2:1 further reduces the crystallite size to 38 nm. Crystallite growth depends on the amount of Co_3O_4 available and the presence of organic agent. Thus, the evolution of gaseous products of the precursor – organic agent reaction disrupts the integrity of the newly formed spinel nanocrystals. The observed decrease in *Lc* values after using an organic impregnation agent is in accordance with the results of the literature (Zavyalova et al., 2007).

The value of the Co_3O_4 lattice parameter a is around 0.808 (Table 1) for all catalysts, implying that the shape and size of the Co_3O_4 unit cell are unchanged by organic-assisted impregnation.

The specific surface of the foam substrate was previously reported to be 0.7 m^2/g (Pacultová et al., 2020). The specific surface of the prepared catalysts was twice larger, 1.9–2.2 m^2/g. The catalyst-specific surfaces were recalculated to find the specific surface of the active Co_3O_4 phase based on its weight fraction in the catalyst. Both the measured and calculated values are presented in Table 1.

For the low-content catalysts, recalculated Co_3O_4 surface areas were found in the range 35–45 m^2/g in the order: $L(Cit) > L(Ure) \approx L(c.i.) > L(Ace) \approx L(Glr) \approx L(Gly)$. Interestingly, the active phase of the catalyst prepared by conventional impregnation shows a similar specific surface, despite having the twice larger crystallite size as calculated from XRD. Although smaller crystallites may generally lead to larger specific surfaces, this may be offset by their agglomeration on the support surface. For the high-content catalysts, the conventionally impregnated catalyst exhibits an active phase specific surface area of 15 m^2/g, while

Table 1
Basic physicochemical properties of the prepared supported catalysts.

	L(c.i.)	*L(Ace)*	*L(Cit)*	*L(Glr)*	*L(Gly)*	*L(Ure)*	*H(c.i.)*	*H(Glr-1)*	*H(Glr-2)*
$w_{Co_3O_4}$(wt.%)	3.1	3.2	3.4	3.2	3.2	3.1	5.5	5.9	6.1
l_c(nm)	60	51	34	32	32	31	148	81	38
a(nm)	0.8084	0.8085	0.8082	0.8082	0.8080	0.8078	0.8084	0.8090	0.8084
S_{BET}($m^2\ g^{-1}$)	1.9	1.8	2.2	1.8	1.8	1.9	1.5	2.2	2.2
$S_{Co_3O_4}$(m^2/g)*	39	35	45	35	35	39	15	26	25

*Calculated from the difference of S_{BET} of supported and pure foam.

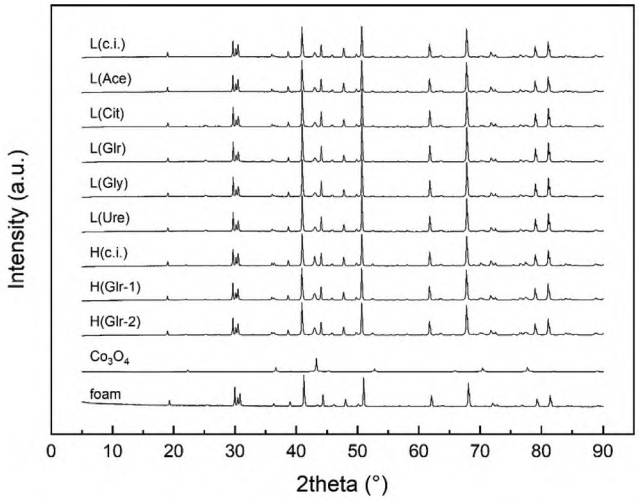

Fig. 1. XRD diffractograms of the Co_3O_4 catalyst prepared by organic-assisted impregnation. Ascription of the peaks to individual phases can be found in Supplementary materials (Table S2).

for both glycerol-impregnated catalysts, the value around 26 m^2/g was found despite the different crystallite sizes. Higher active phase loading, therefore, leads to both larger crystallinity and smaller specific surface area of the active phase.

SEM micrographs of the prepared catalysts taken with a backscattered electron detector are shown in Figs. 2 and 3. Because of the higher atomic number of cobalt compared to the other elements present in the ceramic foam, it appears as bright features. On the low-content catalysts, different active phase morphologies are observed, depending on the organic agent used. It should be stressed that the relative weight of the active components is the same on all of these catalysts. On *L(Cit) and L(glr)*, the active phase forms a continuous layer that covers most of the support surface and is disrupted by craters and cracks. It must be added that for the *L(grl)* catalyst, the places not covered by the active phase were also observed by SEM (S3). On *L(Gly)*, a thin layer covering only parts of the surface is observed, whereas on the rest of the samples clusters of different sizes are scattered over the support surface without any formation of continuous layer similarly to *L(c.i.)* sample.

On the conventionally impregnated high spinel content catalyst (Fig. 3), scattered clusters of the active phase are present similarly to the low spinel content catalyst; in this case, the clusters are larger. On the high spinel content catalysts prepared by glycerol-assisted impregnation, part of the surface is covered by a layer disrupted with cracks; more compact and smoother layer is formed when a higher amount of glycerol was used for the synthesis. The lower values of specific surface observed in the high spinel content catalysts can be explained by a higher agglomeration of the active phase.

More detailed imaging of the catalyst particles can be observed by TEM (S4). The results of the particle size analysis for three selected samples are presented in Fig. 4. Different synthesis routes lead to different sizes of the spinel nanocrystals. For the nanocrystals synthesized without any organic agent (Fig. 4a) the average size is 67 nm with a standard deviation of 27 nm. For the Co_3O_4 nanocrystals synthesized with glycerol and acetic acid the average size is smaller and equals to 44 ± 13 nm and 48 ± 18 nm, respectively. Furthermore, for samples prepared with glycerol, a more uniform size of particles was achieved in accordance with (Gudyka et al., 2017).

The synthesis route also affects the morphology of the nanocrystals (Fig. 2). For the Co_3O_4 nanocrystals synthesized without addition of the auxiliary agent, the nanocrystals have a rather poorly developed subhedral morphology with many defects (*cf.* Fig. 5a1, a2). Nevertheless, within the polyhedral approximation the shape analysis revealed the following abundance of spinel facets (100) – 44 %, (110) – 31 % and (111) – 25 % (cf. Fig. 5 a3, a4). For the Co_3O_4 nanocrystals synthesized with glycerol, an euhedral habit is well developed and morphological defects were not observed (*cf.* Fig. 5 b1, b2, c1, c2). As can be seen in Fig. 5 b3-b4 and c3-c4, spinel nanocrystals prepared with glycerol do not expose the (110) facet. The abundance of the planes (100) and (111) varies from (100) – 65 %, (111) – 35 % for the selected nanocrystal shown in Fig. 2b3 – b4, to (100) – 40 %, (111) – 60 % for that shown in Fig. 2 c3 – c4. The cobalt spinel nanocrystals synthesized with acetic acid (Fig. 5, d3, d4, e3, e4) expose preferentially the (111) plane (73 %) along with the (100) termination (27 %). The effect of the organic agent on the abundance of specific planes was previously published elsewhere (Gudyka et al., 2017; Deganello, 2017).

For all prepared catalysts, a total cobalt spinel reduction was observed during H_2-TPR with the H_2 consumption close to theoretical values, calculated according to the content of the active Co_3O_4 phase (Table 2). The temperatures of the reduction maxima and the total and theoretical H_2 consumption values are presented in Table 2. During Co_3O_4 reduction, two-step reduction: Co^{3+}–Co^{2+}, Co^{2+}-Co^0 is expected (Jacobs et al., 2007; Fratalocchi et al., 2019). The separation of the two steps observed in the reduction profiles is related to the effects of grain size and shape effects (Wójcik et al., 2020). In the reduction profiles presented in Fig. 6, the peak separation is manifested as a single peak with low-temperature shoulder. For the catalyst prepared by conventional impregnation (both *L* and *H* series), the low-temperature shoulder cannot be well distinguished similarly to the *L(Ace)* sample.

For the low-content catalysts, the reduction onset is observed around 220 °C for all catalysts. The reduction maximum is around 360 °C for the *L(c.i.), L(Ace), L(Glr), L(Gly)* samples, while for the *L (Cit), L(Ure)* ones it is shifted to somewhat higher temperatures (371, 390 °C respectively). The total reduction is observed around 460 °C for the *L(c.i.), L(Ace), L(Glr), L(Ure)* catalysts, and around 500 °C for *L(Cit), L(Gly)*. No reduction was observed at higher temperatures. However, in general, changes in the reducibilities of the samples are very gentle.

For the high spinel content catalysts, the reduction onset is also observed around 220 °C for all catalysts. The reduction maximum is at 393 °C for the conventionally impregnated catalyst; for the two glycerol-impregnated catalysts it is shifted towards lower temperatures. The total reduction is observed around 500 °C for the conventional-impregnated catalyst and around 550 °C for the two glycerol-impregnated ones. However, most species are reducible below 450° C. Overall, compared to low spinel content catalysts, while an increase in the amount of reducible species is observed, those are mostly reducible at higher temperatures. This agrees with the higher crystallinity, lower specific surfaces, and higher agglomeration observed by XRD, BET, and SEM, respectively.

3.3. N_2O catalytic decomposition

The prepared catalysts were tested in N_2O decomposition, and the obtained N_2O conversions are presented in Figs. 7 and 8. For the low-spinel content catalysts, the conversions obtained are close to each other, with the *L(Grl)* sample having the highest conversions, and the L(c.i.) one having the lowest. For the high-spinel content catalysts, both conversions and specific rate constants, evaluated according to (Pacultová et al., 2020), follow the same order: *H(Glr-1) > H(Glr-2) > H(c.i.)*. Therefore, for low- and high-

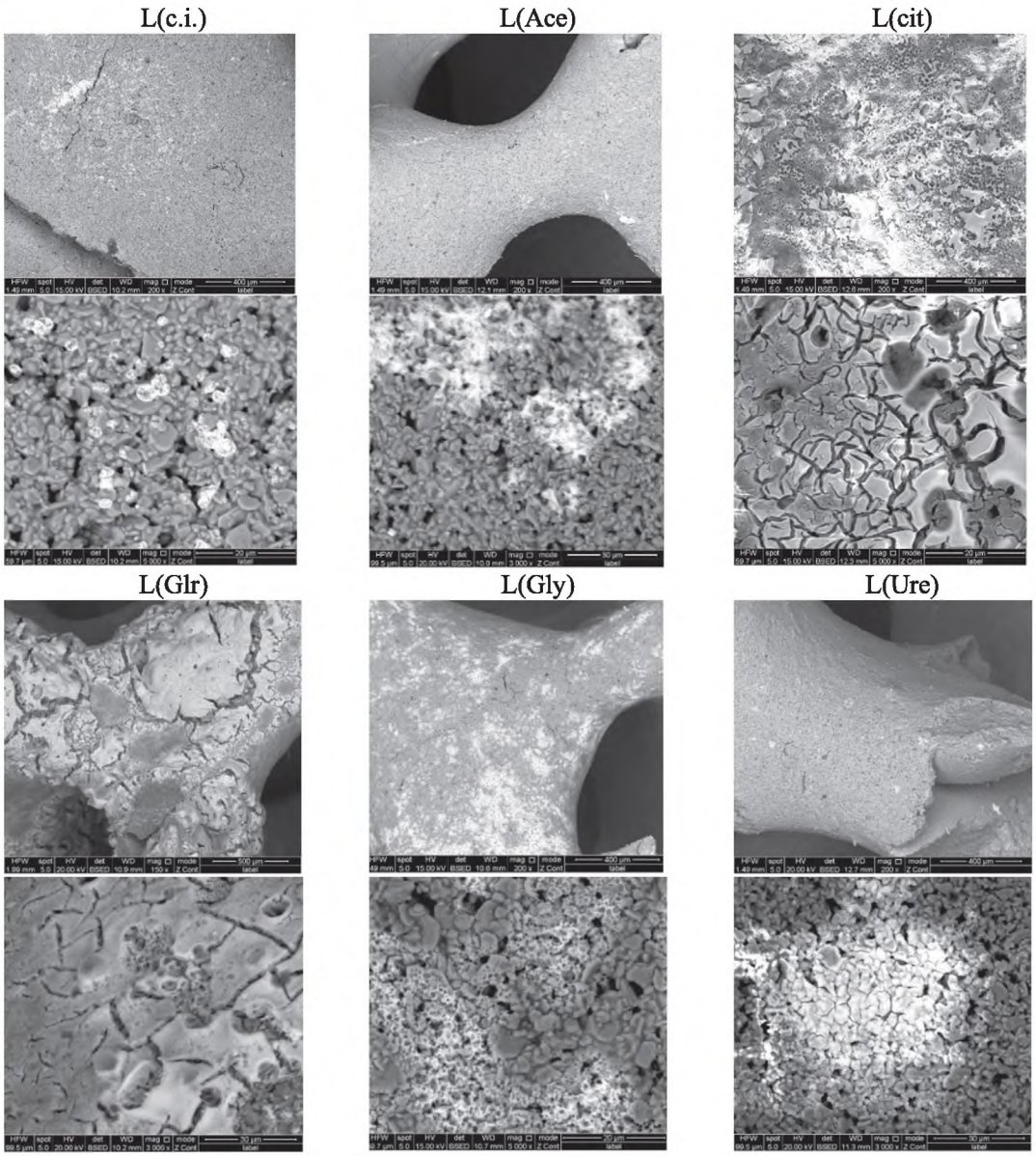

Fig. 2. SEM micrographs of the prepared catalysts of L series.

spinel content catalysts alike, the use of glycerol as the impregnation agent in the ratio 1: 1 leads to the most active catalyst.

3.4. Effect of cesium loading

The catalysts prepared by glycerol-assisted impregnation were the most active of the tested catalyst series, although the differences were not very high. Another reason to use glycerol is the fact that the main drawback of the fuel such as urea or glycine is that hazardous compounds such as NH_3 or NO_x are formed during synthesis, and moreover, according to the literature, carboxylic groups are able to complex most metal cations. However, complexes with alkaline earth cations are less favorite, while hydroxyl groups are more convenient for this purpose (Deganello and Tyagi, 2018). Therefore, we chose glycerol as the impregnation agent used for the cesium amount optimization process. For this purpose, two sets of catalysts with different amounts of cesium were prepared. The first was prepared by conventional impregnation, and the second was prepared by using glycerol as the impregnation agent, while maintaining the molar ratio of the cobalt to glycerol 1:1. The H(c.i.) sample prepared by conventional impregnation without cesium serves as the reference sample for the conventionally prepared series (c.i.) and the H(Glr) sample serves as the reference sample without cesium for the series prepared by glycerol-assisted impregnation. Moreover, the parent solution was used for the preparation of a powder catalyst to compare the effect of cesium on the activity in comparison to the bulk powdered samples as well.

4. Catalysts preparation and characterization

Table 3 shows the basic properties of the supported prepared catalysts such as weight content of the active phase, crystallite size and lattice parameter of the active phase, and Cs weight content of the active phase prepared by conventional and glycerol-assisted impregnation. The weight increment due to active phase deposition is about 6 wt%, only for the C.i.(Cs5) and C.i.(Cs6) samples was slightly lower; about 5 wt%. The amount of Cs promoter pre-

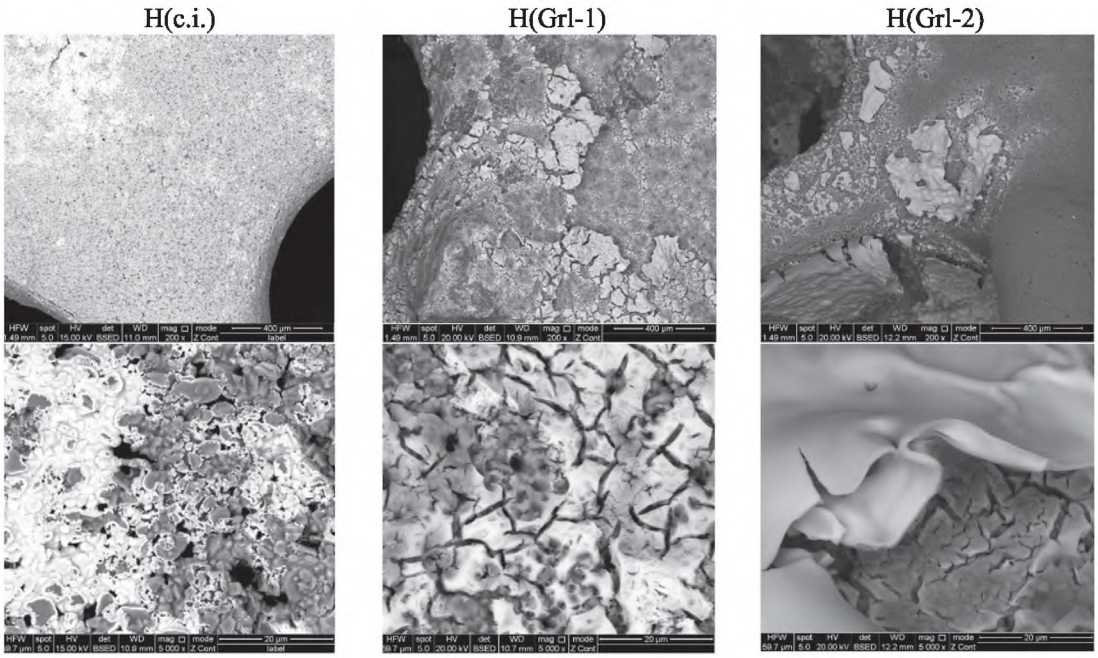

Fig. 3. SEM micrographs of the prepared catalysts H(Grl) series.

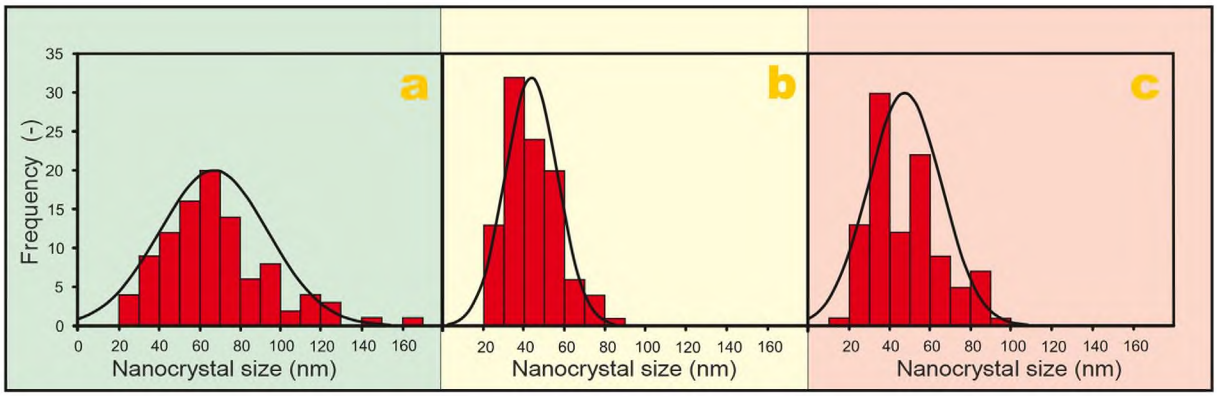

Fig. 4. Particle size analysis of the samples a) L(c.i.) b) L(grl) c) L(ace).

sent in the active phase is somewhat lower for the catalysts prepared by glycerol-assisted impregnation. This is likely caused by an increase in Cs vaporization during calcination due to the temperature increase resulting from the exothermic combustion synthesis reaction of active phase precursors with glycerol (Deganello and Tyagi, 2018; Pacultová et al., 2017).

XRD diffractograms (not shown) show no differences among the catalysts. Again, in all catalysts, a phase corresponding to cobalt spinel oxide (ICDD PDF-2 00–042-1467) was detected. In the supported samples, also the corundum (Al_2O_3) (01–075-1862) and mullite ($Al_{4.54}Si_{1.46}O_{9.73}$) (01–079-1456) phases present in the foam support were observed. Cs-containing phases could not be detected because of their low content in the catalyst. Conventional impregnation leads to crystallite close to the value of sample without Cs that is the *H(c.i.)* sample, while glycerol-assisted impregnation leads to remarkably lower values ranging from 46 to 19 nm (Table 1). The value of the Co_3O_4 lattice parameter was lower for catalysts prepared by glycerol-assisted impregnation and did not change significantly within the individual series. The results show clear structural differences between the two series, however, no effect of cesium loading on structural properties was observed.

Due to low Cs content no cesium phase can be observed by XRD measurement, however as expected for an alkali metal, the only common oxidation state is + 1 as was also confirmed by our previous XPS measurement (Klegova et al., 2022).

The TPR-H_2 results of all samples containing cesium (S5) are very similar to each other (Table 4), however for the *Glr*(Cs) catalyst series the low temperature maximum is shifting more obviously to lower temperatures with increasing Cs loading and the profiles become more flat.

TEM was used to evaluate the location and distribution of Cs in the selected samples. We assumed that Cs can be placed on the support and on the Co_3O_4 phase, noting that the spreading of cesium and potassium and differences in their surface redistribution between the spinel and the support was published previously in (Ciura et al., 2017). On the other hand, the Co:Cs ratio can also be influenced by different cobalt oxide microstructures formed after glycerol is used as an impregnation agent. By elemental STEM-EDX analysis we obtained the Co:Cs ratio for places, where Co_3O_4 is also found (Table 5, S6-S7). Analysis has shown that the Co:Cs ratio decreases in both series with increasing cesium content as expected; however, the values are much higher than those used

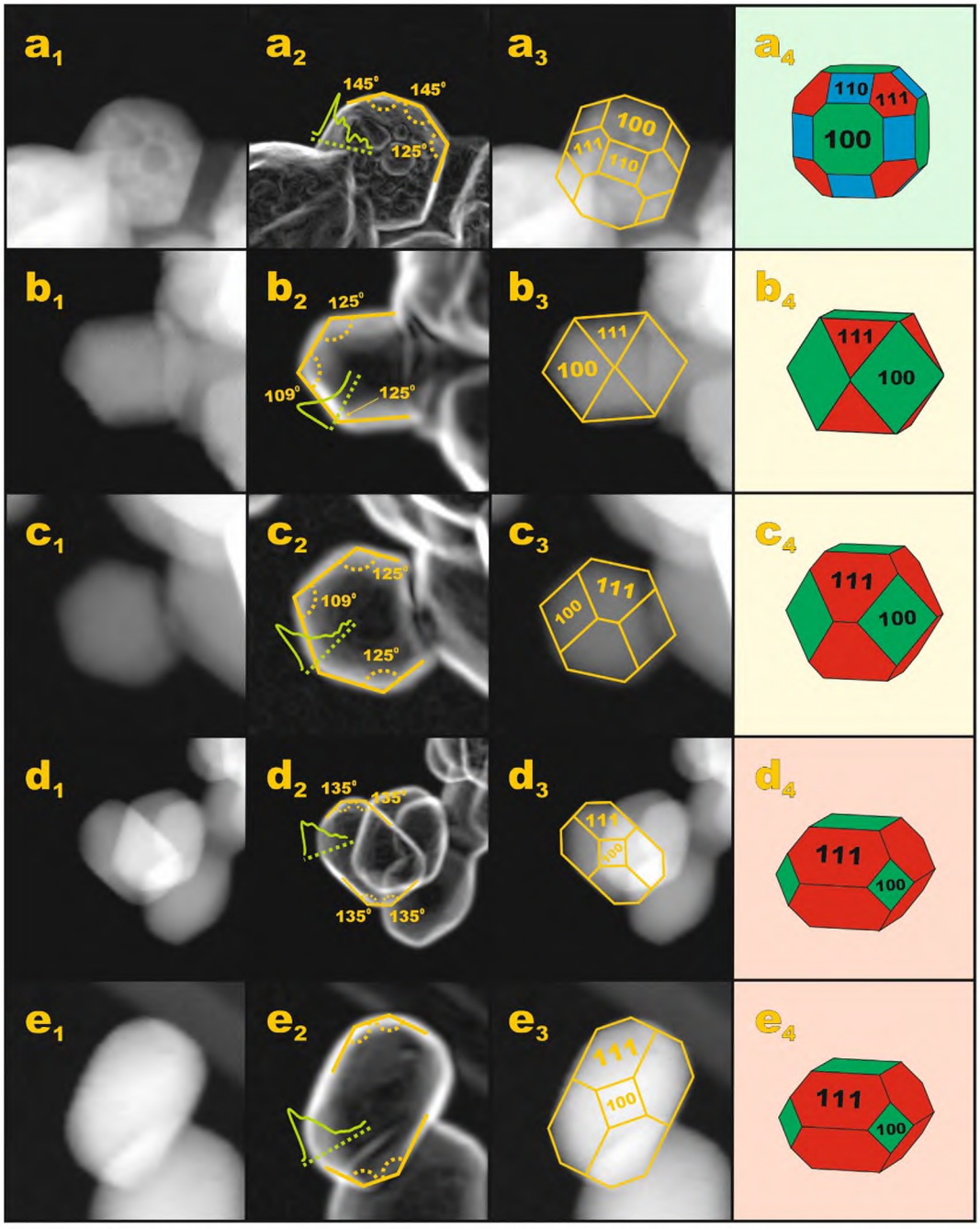

Fig. 5. Shape analysis of the samples a) L(c.i.) b-c) L(grl) and d-e) L(ace). The analysis was based on HAADF STEM (row a_1 – e_1) and the following: contrast gradient analysis (row a_2 – e_2) the images, edge patterns superimposed with HAADF STEM images (row a_3 – e_3) and the retrieved Wulff shape of the nanocrystals (row a_4 – e_4).

Table 2
TPR-H_2 temperatures of reduction maxima, experimental and theoretical H_2 consumption.

	L(c.i.)	*L(Ace)*	*L(Cit)*	*L(Glr)*	*L(Gly)*	*L(Ure)*	*H(c.i.)*	*H(Glr-1)*	*H(Glr-2)*
T_{max}(°C)*	363	362	371	359	360	390	393	371	378
H_2 consumption (mmol g^{-1})	0.6	0.5	0.7	0.6	0.6	0.7	1.0	1.0	1.1
Theoretical H_2 consumption (mmolg^{-1})	0.5	0.5	0.6	0.5	0.5	0.5	0.9	1.0	1.0

*Experimental error ± 5 °C.

for catalyst preparation (nominal content molar ratio). They are also higher than the values obtained from AAS, with the exception of the Glr(Cs1) sample, where comparable results were obtained. Higher values mean that part of the cesium must be located on the support without any contact with the Co_3O_4 phase. We tried to confirm the suggestion that Cs is placed on the support solely by STEM-EDX. Cesium presence on the support was observed on the *C.i. (Cs6)* and *Glr (Cs3)* samples. Surprisingly, we did not observe

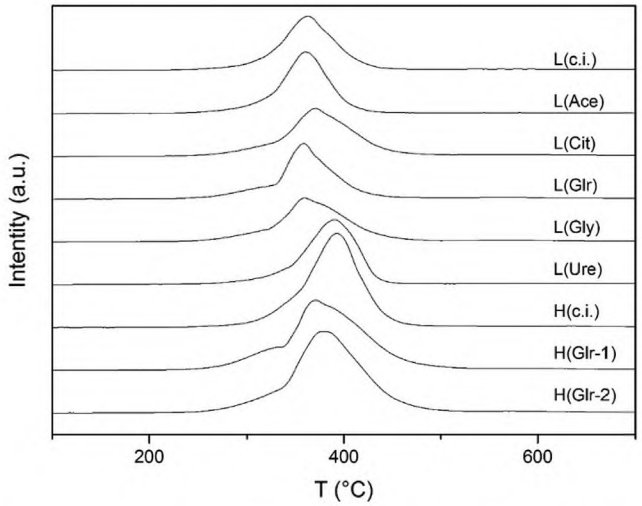

Fig. 6. TPR-H_2 profiles of the prepared catalysts using different organic agents.

it on the selected support locations of *C.i. (Cs4)* and *Glr (Cs6)* samples. Since we saw clear inhomogeneity of support composition, we suppose that inhomogeneity of Cs placement on the support is connected to the inhomogeneity of the support.

4.1. N_2O catalytic decomposition

The prepared catalysts were tested for nitrous oxide decomposition to compare the effect of Cs content on catalytic activity in the bulk cobalt active phase and in the active phase deposited on the ceramic support by conventional and glycerol-assisted impregnation. The aim was to find an optimal Cs loading in the cobalt-based catalyst deposited on the ceramic foam for N_2O decomposition. Different cesium loadings strongly influenced the catalytic activity of all samples; however, the results were different for the each of the examined series. N_2O conversion under inert conditions for bulk and conventionally impregnated samples is shown in Figs. 9 and 10a, respectively. The optimal cesium range for the bulk samples is wider for higher temperatures, yet it is very narrow and lies between 0.5 and 1.4 wt%. This finding agrees with the results for cesium-doped spinels prepared from cobalt nitrate using different precipitating agents (Michalík et. al., 2017), where the optimum of 1 wt% was found. The optimal cesium loading shifts to 2–3 wt% after the deposition of the active phase on the foam support by conventional impregnation (Fig. 10a) and the window is markedly enlarged to 1–3 wt% for samples prepared by glycerol-assisted impregnation (Fig. 10b).

Obvious differences in catalytic activity for the two supported samples can be observed in the streams simulating off gases from nitric acid plats, that is containing besides 1000 ppm of N_2O also 5 mol.% O_2, 2 mol.% H_2O and 200 ppm NO (Fig. 11. and 12). The positive influence of glycerol is even stronger, resulting not only in the wide range window of the optimal cesium loading compared to that of the catalyst prepared by conventional impregnation but also in conversion increase especially at low temperatures.

Regarding comparison the activity results with results from scientific literature, it must be noticed, that mostly unsupported catalysts were tested and presented and these cańt be applied at industrial level. The newest results obtained using structured foam catalysts was published by Ho (Ho et al., 2022), who also showed nice comparison for Co containing catalysts reported in the literature, showing his catalyst as very active. Anyway, the results shown in Fig. 12 b) are the best among shaped catalysts designed for N_2O decomposition. Direct comparison of conversion is difficult due to different conditions used but keeping in mind the difference in GHSV applied rough comparison can be obtained. We have achieved 75 % conversion at 420 °C and almost 100 % at 450 °C at GHSV = 1500 h^{-1} in the presence of O_2, NO and H_2O, while Ho achieved almost zero conversion at 420 °C and<30 % at 450 °C at GHSV = 3500 h^{-1} in the presence of O_2 and NO. The results confirm that Co_3O_4-Cs deposited on an open cell ceramic foam as catalysts for N_2O decomposition are a promising alternative to conventional fixed-bed reactors.

5. Discussion

The fact that the amount of cesium (expressed as atoms of Cs/nm^2 or wt. % of Cs (Ciura et al., 2017) or Co/Cs determined from XPS (Klegova et al., 2022) is crucial for the activity of the Co_3O_4 catalyst is generally known (Wójcik et al., 2020). Comparing our activity results, we see that there is a difference between unsupported bulk samples and supported one, and moreover, there are also differences between supported samples prepared by different procedures if the comparison is based on the nominal values of Co/Cs set during preparation. At first sight, it seems that the optimal ratio of Co/Cs is different for each set of the catalysts.

However, after evaluation of the Co/Cs ratio by TEM only on the regions where the support is covered by a spinel active phase, a connection between the behavior of the catalysts can be established. Considering that in the powdered catalyst all samples work

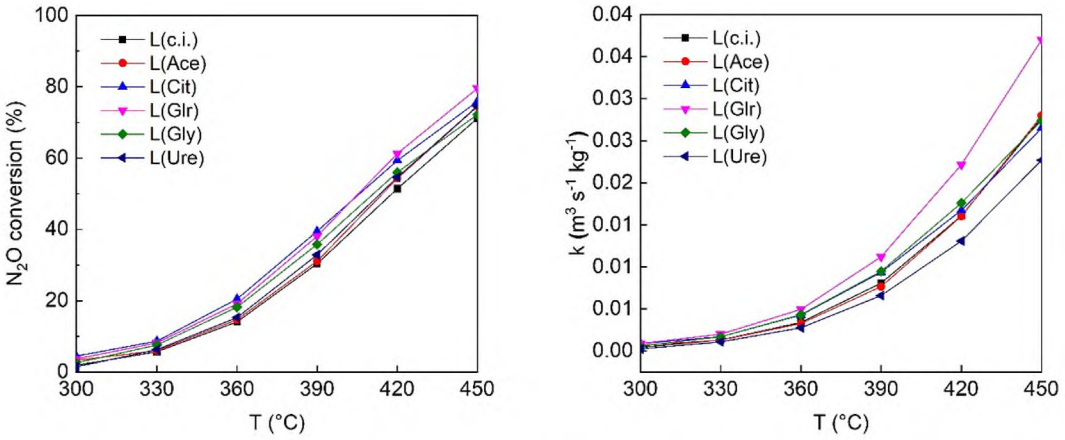

Fig. 7. N_2O conversion and kinetics constants of the prepared catalysts. Conditions: 0.1 mol. % N_2O in N_2, GHSV (20 °C, 101325 Pa) = 1080 $m^3h^{-1}m_{cat}^{-3}$.

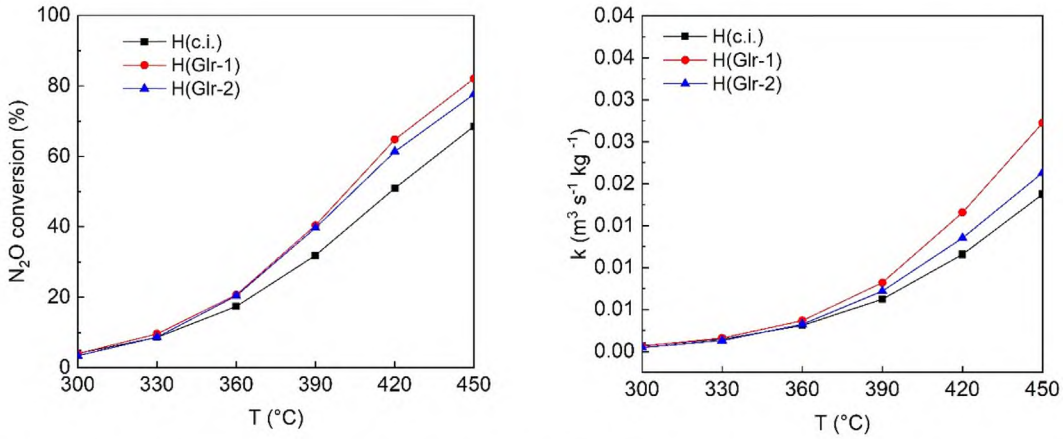

Fig. 8. N_2O conversion and kinetics constants of the prepared catalysts. Conditions: 0.1 mol. % N_2O in N_2, GHSV (20 °C, 101325 Pa) = 1500 $m^3h^{-1}m^{-3}_{cat}$.

Table 3
Basic physicochemical properties of catalysts prepared by conventional impregnation and glycerol assisted impregnation differing in cesium loading.

Sample	*C.i.(Cs1)*	*C.i.(Cs2)*	*C.i.(Cs3)*	*C.i.(Cs4)*	*C.i.(Cs5)*	*C.i.(Cs6)*
Cs-Co_3O_4 (wt. %)	5.5	5.9	6.7	6.0	4.4	4.7
L_c (nm)	151	207	162	133	n.d.	n.d.
a (nm)	0.8082	0.8084	0.8081	0.8083	n.d.	n.d.
Cs (wt.%)*	0.7	1.4	2.1	2.7	3.6	3.8
Sample	*Glr(Cs1)*	*Glr(Cs2)*	*Glr(Cs3)*	*Glr(Cs4)*	*Glr(Cs5)*	*Glr(Cs6)*
Cs-Co_3O_4 (wt. %)	5.7	5.5	5.1	6.2	5.9	5.8
L_c (nm)	46	19	22	20	19	24
a (nm)	0.8073	0.8076	0.8080	0.8079	0.8078	0.8077
Cs (wt.%).	0.6	1.0	1.5	1.9	2.5	3.0

* wt. % related toCo_3O_4 calculated from AAS results and known weight of deposited active phase.

Table 4
TPR-H_2 temperatures of reduction maxima, H_2 experimental and theoretical consumption of catalysts prepared by conventional impregnation and glycerol assisted impregnation differing in cesium loading.

Sample	*C.i.(Cs1)*	*C.i.(Cs2)*	*C.i.(Cs3)*	*C.i.(Cs4)*	*C.i.(Cs5)*	*C.i.(Cs6)*
$T_{max,1}$ *	–	–	336	327	–	–
$T_{max,2}$ *	383	371	375	381	372	385
Exp. H_2	1.1	1.1	1.2	1.0	0.8	0.8
Theor. H_2	0.9	1.0	1.1	1.0	0.7	0.8
Sample	*Glr(Cs1)*	*Glr(Cs2)*	*Glr(Cs3)*	*Glr(Cs4)*	*Glr(Cs5)*	*Glr(Cs6)*
$T_{max,1}$ *	325	324	319	312	304	300
$T_{max,2}$ *	361	370	372	373	370	365
Exp. H_2	1.1	1.0	0.9	1.1	0.9	0.9
Theor. H_2	1.0	0.9	0.9	1.0	1.0	1.0

*Experimental error ± 5 °C.

Table 5
Analysis of the elemental composition of supported spinel nanocrystal samples prepared without and with the active agent – glycerol.

Sample	Co:Cs molar ration from STEM-EDX *	Co:Cs molar ration nominal content	Co:Cs molar ration from AAS
C.i.(Cs4)	161	38	53
C.i.(Cs6)	57	25	42
Glr(Cs1)	249	150	267
Glr(Cs3)	192	50	111
Glr(Cs6)	79	25	54

*Measured on the spinel.

in the kinetic region (Obalová et al., 2019), and cesium is distributed homogeneously on the cobalt spinel phase, we can obtain the Co/Co molar ratio from the AAS analysis. From Fig. 9 the optimal cesium range is 0.5–1.4 wt% of Cs. Recalculating the wt.% values to the Co/Cs molar ratio on the basis of relation obtained from Fig. S8, gives the region of Co/Cs molar ratio of 244–91. The values represent the real molar ratio, which is necessary for an optimal catalyst performance (marked as the blue region in Fig. S9 and S10). For the supported samples, we know the Co/Cs values for the selected samples obtained from TEM analysis in the places where the spinel active phase is present. Giving these values to the relation with the nominal amount of cesium, we obtain the optimal nominal content of cesium for supported catalysts prepared by the conventional impregnation (2.4–5.3 wt%, Fig. S9 left, green region) and supported catalysts prepared by glycerol-assisted impregnation (1.1–5.8 wt%, Fig. S9 right, red region). The regions differ for both types of the catalysts. These values can be easily converted to the optimal cesium content determined by AAS (Fig. S10). For the samples prepared by conventional impregnation, it gives the region of optimal performance being 1.6–3.5 wt% of Cs (AAS) and for catalysts prepared by glycerol-assisted impregnation it is 0.6–2.9 wt% of Cs (AAS). Comparing

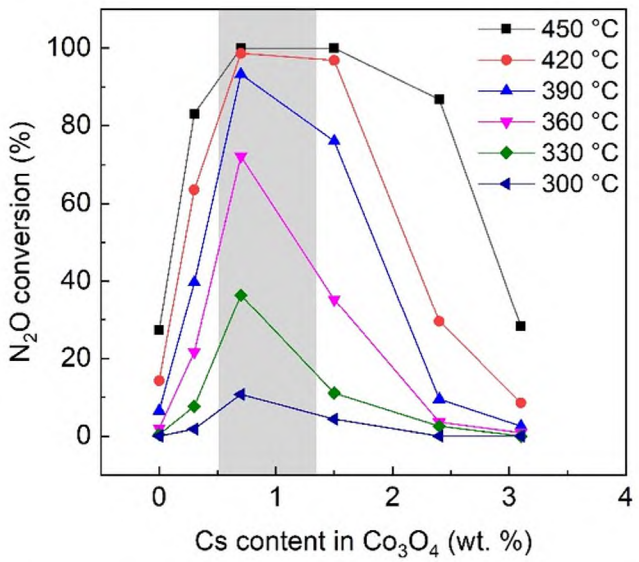

Fig. 9. Dependence of N_2O conversion on the Cs content in Co_3O_4 over bulk active phase. Conditions: 1000 ppm N_2O in N_2, GHSV = 60 L $g^{-1}h^{-1}$. Cs wt. % are related to Co_3O_4 calculated from AAS results and known weight of deposited active phase.

the data with catalytic results shown in Figs. 10-12, good agreement is obtained. The reasons for such behavior can be deduced from the preparation procedure and the microstructural characterization observable by SEM and TEM. What is clearly shown is that cesium must be in tight contact with cobalt spinel phase to ensure catalytic performance. Thus, every deposition procedure used for the active phase deposition on the support resulting in the non-ideal coverage of the support by the cobalt spinel phase will lead to the situation where part of the used cesium promoter will be placed on the support without contact with the spinel phase, and this is why such cesium species will not take part in the reaction. As it was shown (SEM, TEM) using the organic impregnation agents ensures better spreading of the cobalt oxide phase on the support, and thus leaves less space on the bare fragments of the support for depositing the isolated cesium species. Generally, glycerol exhibits a high viscosity, which favors a more uniform metal distribution on the support during the drying step (Zavyalova et al., 2009). This explains especially the shape of the N_2O conversion dependence at the side of the low cesium content, where the samples prepared by glycerol-assisted impregnation and low cesium content (around 1 wt%) are more active than the conventionally impregnated samples. However, better contact of the cesium and cobalt oxide entities can also be the result of the complexing ability of glycerol for the cobalt and cesium ions in the solution and during the subsequent drying step, when gelation of the solution is expected. According to the literature, cobalt glycerolate was observed during preparation using a solution of water-glycerol and cobalt nitrate (Gudyka et al., 2017). Complexes of glycerol with different metals, including alkali metals, are also known (Lau et al., 2016; Schatte et al., 2011) as well as bimetal glycerolates (Li et al., 2019). For instance, the Mn-enriched surface of the metal-defected spinel was obtained by thermal calcination of manganese and cobalt glycerolates as a result of the formation rate difference between manganese and cobalt glycerolates (Li et al., 2019). For that reason, it can be suggested that some kind of complexes are formed, however, to the best of our knowledge no systematic study exists explaining the effect of the complexes of cobalt and cesium on the resulting homogeneity/dispersion of cation mixing. Anyway, the role of the network is to maintain metal cations homogeneously fixed during the combustion and to prevent selective precipitation of the metal ions during water removal resulting in better dispersion (Deganello and Tyagi, 2018; Varma et al., 2016; Junliang et al., 2009).

The second reason is related to the volatilization of cesium during the preparation process. It is known that during synthesis based on solution combustion methods the local temperature during combustion is much higher than the average temperature in the oven (Deganello and Tyagi, 2018). Cesium can easily volatilize due to elevated temperatures (Pacultová et al., 2017) and for this reason less cesium remained in the supported samples prepared by the glycerol-assisted combustion than in the samples prepared by conventional impregnation (Table 3). The promotional effect of cesium is of an electronic nature (facilitation of the N_2O activation via interfacial electron transfer, $N_2O + e^-(Co^{3+}) \rightarrow N_{2(g)} + O^-_{ads}$), and exceeding the optimal limit ceases this effect, and consequently leads to decrease in the catalytic activity (Wójcik et al., 2020), which is explicitly observed in Fig. 9 for powdered samples. In supported samples, the shape of the conversion dependence on the side of the high cesium content is flatter for samples prepared by glycerol-assisted impregnation due to the lower residual cesium amount of these samples.

The explanations given above provide the reasons for the apparent changes in the optimal amount of cesium for individual sets of

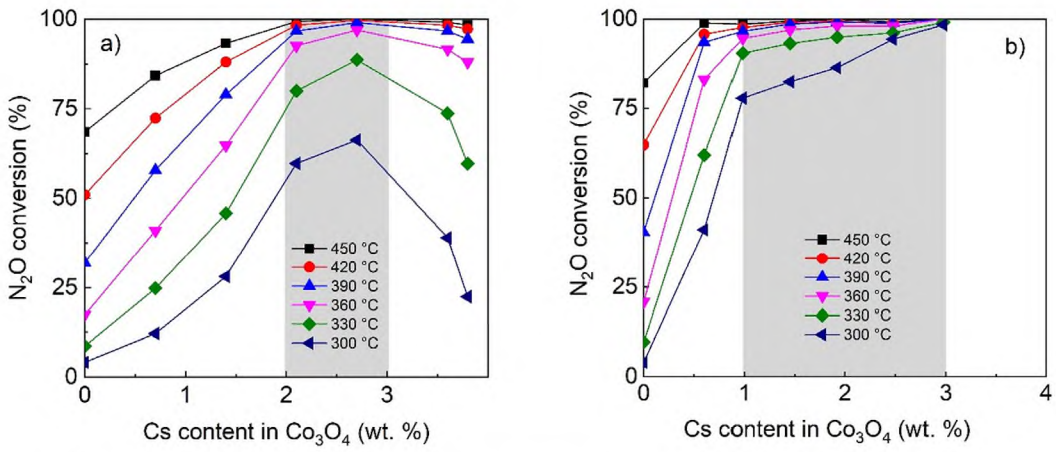

Fig. 10. Dependence of N_2O conversion on the Cs content (AAS) in Co_3O_4 over supported catalysts prepared by a) conventional impregnation b) glycerol assisted impregnation. Conditions: 1000 ppm N_2O in N_2, GHSV (20 °C, 101325 Pa) = 1500 $m^3h^{-1}m^{-3}_{cat}$. Cs wt. % are related to Co_3O_4 calculated from AAS results and known weight of deposited active phase.

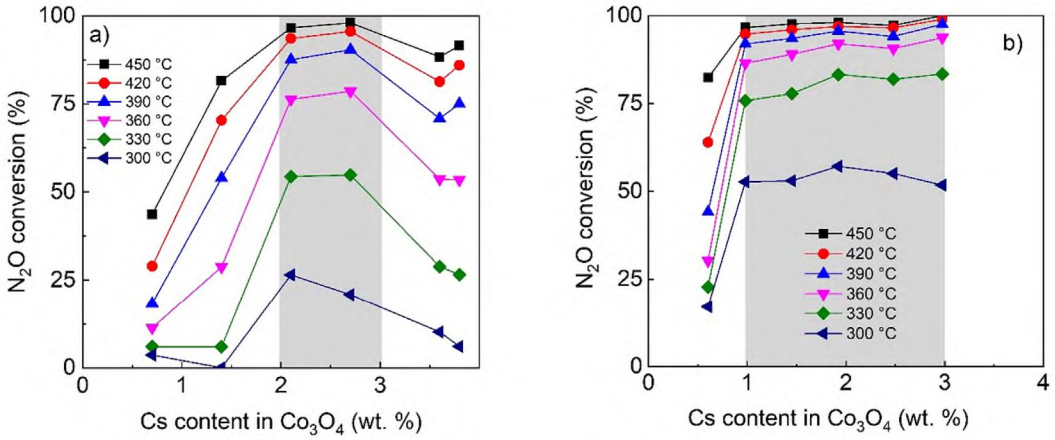

Fig. 11. Dependence of N_2O conversion on the Cs content (AAS) in Co_3O_4 over supported catalysts prepared by a) conventional impregnation b) glycerol assisted impregnation in the presence of oxygen and water vapor. Conditions: 1000 ppm N_2O in N_2 + 5 mol.% O_2 and 2 mol.% H_2O, GHSV (20 °C, 101325 Pa) = 1500 $m^3h^{-1}m_{cat}^{-3}$. Cs wt. % are related to Co_3O_4 calculated from AAS results and known weight of deposited active phase.

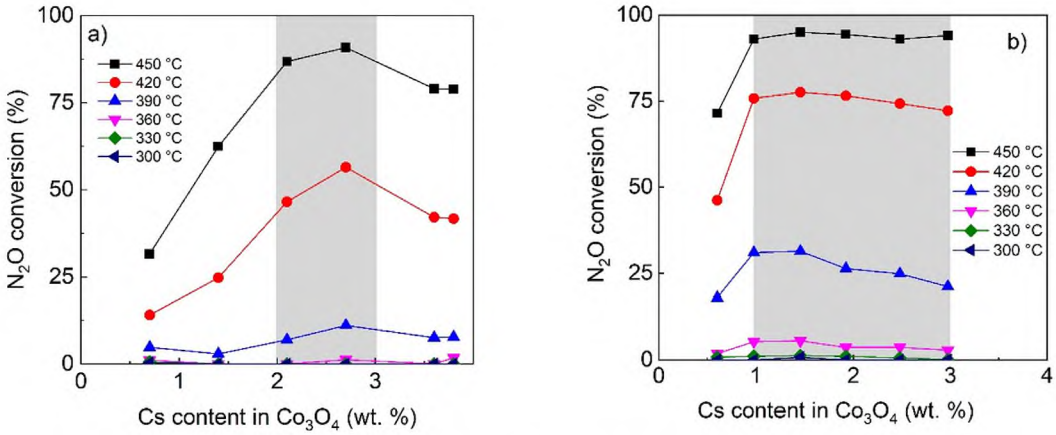

Fig. 12. Dependence of N_2O conversion supported catalysts on the Cs content (AAS) in Co_3O_4 prepared by a) conventional impregnation b) glycerol assisted impregnation in the presence of oxygen, water vapor and NO. Conditions: 1000 ppm N_2O in N_2 + 5 mol.% O_2, 2 mol.% H_2O and 200 ppm NO, GHSV (20 °C, 101325 Pa) = 1500 $m^3h^{-1}m_{cat}^{-3}$. Cs wt. % are related to Co_3O_4 calculated from AAS results and known weight of deposited active phase.

the samples. However, in addition to this, we also observed an increase in activity for the samples prepared by glycerol-assisted impregnation, even comparing only those samples that had an optimal amount of cesium. The observed features must be related to changes in the morphology (faceting) of the spinel crystallites supported on the ceramic foam. In our case, the use of glycerol lead to complete disappearance of the exposed (110) planes, and the consequent increased abundance of (100) or (111) facets. The predomination of the (100) facets after glycerol assisted deposition of cobalt spinel on the Al_2O_3 support has also been documented elsewhere (Gudyka et al., 2017), in accordance with our results. However, an effect on the abundance of (110) planes has not been noted therein. The increased catalytic deN_2O activity has been explained by the lower content of the surface coordinatively unsaturated ions and the resultant much higher resistance of the (100) plane to poisoning by H_2O and NO_x. A deeper elucidation of this issue has been provided on the basis of ab initio thermodynamic modelling, where pronounced differences in the blocking efficiency of the surface cobalt sites located on the (100) and (110) facets by O_2, H_2O and NO, depending on temperature has been discussed in detail (Grzybek et al., 2021; Zasada et al., 2010). Looking at our catalytic results, one can see that the differences in the N_2O conversion of the samples containing an optimum amount of cesium between the supported samples prepared by conventional and glycerol-assisted impregnations are observed below 330 °C for the inert conditions and below 390 and 420° C in the presence of oxygen and water vapor or in oxygen, water vapor and nitric oxide together, respectively. Following Zasada et al. (Grzybek et al., 2021; Zasada et al., 2010; Zasada et al., 2020) for the (100) facet the desorption of the contaminants takes place around 380 °C for oxygen, 270 °C for H_2O and 400 °C for NO. These are also the temperatures below which we observed a positive effect of glycerol.

6. Conclusions

Co_3O_4 active phase was deposited on a ceramic foam support using conventional and organic-assisted impregnation method. All the catalysts ensured higher N_2O conversion then conventionally impregnated catalyst. Regardless of the impregnation agent used, the active phase consisted from Co_3O_4 with similar values of lattice parameter *a* and comparable reducibility. However, the different organic impregnation agents influenced the morphology of the active phase thus influencing its agglomeration and the specific surface area. Moreover organic-assisted impregnation lead to a higher abundance of smaller particles and different faceting compared to conventional impregnation. Using organic agent caused decline of the (110) and increase of the (100) and (111) facets abundances.

The optimal amount of Cs in Co_3O_4 deposited on the ceramic foam is approximately 2–3 times higher than in the case of bulk Co_3O_4-Cs. The difference is explained by dispersion of part of the Cs species over pure support (places not covered by Co_3O_4), thus changing the Cs and Co_3O_4 that are in the real contact and only these species participate in the reaction and influence catalytic activity. The Co:Cs molar ratio, which is necessary for optimal catalyst performance, was found to be 90–250, however to reach this "real contacting" ratio, different starting conditions must be used according to the selected preparation method. The advantage of the use of glycerol during impregnation lies in the fact that (i) the complexation of the Co^{2+} and Cs^{+} cations ensures better contact between cesium and cobalt,(ii) surface is better covered by the spinel phase, thus leaving less space to spread the cesium on the support rather than in the spinel phase and therefore wider concentration range of Cs can be used during preparation and (iii) refaceting of the spinel nanocrystals with preferential exposure of the (100) planes takes place which causes higher resistance against H_2O, O_2 and NO contaminants, typically present in the real gases.

Declaration of competing interest

The authors declare that they have no known competing financial interests or personal relationships that could have appeared to influence the work reported in this paper.

Acknowledgement

The work was supported from ERDF "Institute of Environmental Technology – Excellent Research" (project No. CZ.02.1.01/0.0/0.0/16_019/0000853). Experimental results were accomplished by using Large Research Infrastructure ENREGAT (No. LM2018098) supported by the Ministry of Education, Youth and Sports of the Czech Republic. Authors thank Lanik company (Czech Republic) for ceramic foams.

Appendix A. Supplementary data

Supplementary data to this article can be found online at https://doi.org/10.1016/j.arabjc.2023.105311.

References

Bera, P., 2019. Solution Combustion Synthesis as a Novel Route to Preparation of Catalysts, International Journal of Self-Propagating High-Temperature. Synthesis 28, 77–109.
Canny, J., 1986. A computational approach to edge detection. IEEE Trans. Pattern Anal. Mach. Intelli. PAMI-8, 679–698.
Ciura, K., Grzybek, G., Wójcik, S., Indyka, P., Kotarba, A., Sojka, Z., 2017. Optimization of cesium and potassium promoter loading in alkali-doped $Zn_{0.4}Co_{2.6}O_4|Al_2O_3$ catalysts for N_2O abatement. React. Kinet. Mech. 121, 645–655.
Ciura, K., Grzybek, G., Wójcik, S., Indyka, P., Kotarba, A., Sojka, Z., 2017. Optimization of cesium and potassium promoter loading in alkali-doped $Zn_{0.4}Co_{2.6}O_4|Al_2O_3$ catalysts for N_2O abatement. React. Kinet. Mech. Catal. 121, 645–655.
Deganello, F., 2017. Nanomaterials for environmental and energy applications prepared by solution combustion based-methodologies: Role of the fuel. Mater. Today:. Proc. 4, 5507–5516.
Deganello, F., Tyagi, A.K., 2018. Solution combustion synthesis, energy and environment: best parameters for better materials. Prog. Cryst. Growth Charact. Mater. 64, 23–61.
Digital Micrograph, Gatan Inc. 2007. Digital Micrograph. Pleasanton, California. https://www.gatan.com/products/tem-analysis/digitalmicrograph-software
FeatureJ, M.E., 2003. Biomedical Imaging Group of the Swiss Federal Institute of Technology in Lausanne (EPFL).
Fratalocchi, L., Lietti, L., Visconti, C.G., Fischer, N., Claeys, M., 2019. Catalytic consequences of platinum deposition order on cobalt-based Fischer-Tropsch catalysts with low and high cobalt oxide dispersion. Catal. Sci. Technol. 9, 3177–3192.
Frutos, O.D., 2018. A state-of-the-art review on nitrous oxide control from waste treatent and industrial sources. Biotechnol. Adv., 1025–1037.
González-Cortés, S.L., Imbert, F.E., 2013. Fundamentals, properties and applications of solid catalysts prepared by solution combustion synthesis (SCS). Appl. Catal. A: General, 117–131.
Gryboś, J., Indyko, P., Sojka, Z., 2021. Metal Oxide Nanoparticles: Formation, Functional Properties, and Interfaces. Wiley-Blackwell.
Grzybek, G. et al., 2017. Influence of preparation method on dispersion of cobalt spinel over alumina extrudates and the catalyst deN_2O activity. Appl. Catal. B, 34–44.
Grzybek, G., Wójcik, S., Legutko, P., Gryboś, J., Indyka, P., Leszczyński, B., Kotarba, A., Sojka, Z., 2017. Thermal stability and repartition of potassium promoter between the support and active phase in the $K\text{-}Co_{2.6}Zn_{0.4}O_4|\alpha\text{-}Al_2O_3$ catalyst for N_2O decomposition: crucial role of activation temperature on catalytic performance. Appl. Catal. B 205, 597–6041.
Grzybek, G., Gryboś, J., Indyka, P., Janas, J., Ciura, K., Leszczyński, B., Zasada, F., Kotarba, A., Sojka, Z., 2021. Evaluation of the inhibiting effect of H_2O, O_2, and NO on the performance of laboratory and pilot $K\text{-}Zn_xCo_{3-x}O_4$ catalysts supported on $\alpha\text{-}Al_2O_3$ for low-temperature N_2O decomposition. Appl. Catal. B 297, 120435.
Gudyka, S. et al., 2017. Enhancing the deN_2O activity of the suported $Co_3O_4|a\text{-}Al_2O_3$ catalyst by glycerol-assisted shape engineering of the active phase at the nanoscale. Appl. Catal. B, 339–349.
Ho, P.H., Da Costa, K.Ś., de Luna, G.S., Jabłońska, M., Ospitali, F., Di Renzo, F., Delahay, G., Fornasari, G., Vaccari, A., Palkovits, R., Benito, P., 2022. Facile coating of Co_3O_4 on open-cell metallic foam for N_2O catalytic decomposition. Chem. Eng. Res. Des. 188, 166–178.
Jacobs, G., Ji, Y., Davis, B.H., Cronauer, D., Kropf, A.J., Marshall, C.L., 2007. Fischer-Tropsch synthesis: temperature programmed EXAFS/XANES investigation of the influence of support type, cobalt loading, and noble metal promoter addition to the reduction behavior of cobalt oxide particles. Appl. Catal. A 333, 177–191.
Junliang, L., Wei, Z., Cuijing, G., Yanwei, Z., 2009. Synthesis and magnetic properties of quasi-single domain M-type barium hexaferrite powders via sol–gel auto-combustion: effects of pH and the ratio of citric acid to metal ions. CA/M. J. Alloy. Compd. 479, 863–869.
Kapteijn, F., Rodriguez-Mirasol, J., Moulijn, J.A., 1996. Heterogeneous catalytic decomposition of nitrous oxide. Appl. Catal. B, 25–64.
Klegova, A., Inayat, A., Indyka, P., Gryboś, J., Sojka, Z., Pacultová, K., Schwieger, W., Volodarskaja, A., Kuśtrowski, P., Rokicińska, A., Fridrichová, D., Obalová, L., 2019. Cobalt mixed oxides deposited on the SiC open-cell foams for nitrous oxide decomposition. Appl. Catal. B 255, 117745.
Klegova, A., Pacultová, K., Kiška, T., Peikertová, P., Rokicińska, A., Kuśtrowski, P., Obalová, L., 2022. Washcoated open-cell foam cobalt spinel catalysts for N_2O decomposition. Mol. Catal. 533, 112754.
Klegova, A., Pacultová, K., Kiška, T., Obalová, L., 2023. How loading of Co_3O_4-Cs on an open-cell foam influences N_2O decomposition. Ind. Eng. Chem. Res..
Kočí, K., Reli, M., Troppová, I., Šihor, M., Bajcarová, T., Ritz, M., Pavlovský, J., Praus, P., 2019. Photocatalytic decomposition of N_2O by using nanostructured graphitic carbon nitride/zinc oxide photocatalysts immobilized on foam. Catalysts..
Konsolakis, M., 2015. Recent advances on nitrous oxide (N_2O) decomposition over non-noble-metal oxide catalysts: catalytic performance, mechanistic considerations, and surface chemistry aspects. ACS Catal., 6397–6421.
Lau, P.-C., Kwong, T.-L., Yung, K.-F., 2016. Effective heterogeneous transition metal glycerolates catalysts for one-step biodiesel production from low grade non-refined Jatropha oil and crude aqueous bioethanol. Sci. Rep. 6, 23822.
Li, K., Zhang, R., Gao, R., Shen, G.-Q., Pan, L., Yao, Y., Yu, K., Zhang, X., Zou, J.-J., 2019. Metal-defected spinel $Mn_xCo_{3-x}O_4$ with octahedral Mn-enriched surface for highly efficient oxygen reduction reaction. Appl. Catal. B 244, 536–545.
Meille, V., 2006. Review on methods to deposit catalysts on structured surfaces. Appl. Catal. A, 1–17.
Michalík, S., Pacultová, K., Obalová, L., 2017. In: Cesium Doped Co_3O_4 spinel for N_2O decomposition. Technology (ICCT). Czech Soc. Industrial Chemistry, Prague, Czech republic, Mikulov, Czech Republic, pp. 536–539.
Nitric Acid, Reference Document on Best Available Techniques for the Manufacture of Large Volume Inorganic Chemicals-Ammonia, Acids and Fertilisers, European Commission, Sevilla, 2007, pp. 95-143.
Novitskaya, E., Kelly, J.P., Bhaduri, S., Graeve, O.A., 2021. A review of solution combustion synthesis: an analysis of parameters controlling powder characteristics. Int. Mater. Rev. 66, 188–214.
Obalová, L., Klegova, A., Matějová, L., Pacultová, K., Fridrichová, D., 2019. Must the best laboratory prepared catalyst also be the best in an operational application?. Catalysts 9, 160.
Pacultová, K., Draštíková, V., Chromčáková, Ž., Bílková, T., Kutláková, K.M., Kotarba, A., Obalová, L., 2017. On the stability of alkali metal promoters in Co mixed oxides during direct NO catalytic decomposition. Mol. Catal. 428, 33–40.
Pacultová, K., Klegova, A., Kiška, T., Fridrichová, D., Martaus, A., Rokicinska, A., Kustrowski, P., Obalová, L., 2020. Effect of support on the catalytic activity of Co_3O_4-Cs deposited on open-cell ceramic foams for N_2O decomposition. Mater. Res. Bull. 129, 12.
Pacultová, K., Klegová, A., Kiška, T., Fridrichová, D., Martaus, A., Rokicińska, A., Kuśtrowski, P., Obalová, L., 2020. Effect of support on the catalytic activity of Co_3O_4-Cs deposited on open-cell ceramic foams for N_2O decomposition. Mater. Res. Bull. 129, 110892.
Pérez-Ramírez, J. et al., 2003. Formation and control of N_2O in nitric acid production: where do we stand today?. Appl. Catal. B, 117–151.
Rasband, W.S., Rasband, W.S., 1997. ImageJ; U.S. National Institutes of Health: Bethesda, Maryland. ImageJ.

Ravishankara, A.R., Daniel, J.S., Portmann, R.W., 2009. Nitrous Oxide (N_2O): the dominant ozone-depleting substance emitted in the 21st century. Science, 123–125.
Reli, M., Troppová, I., Šihor, M., Pavlovský, J., Praus, P., Kočí, K., 2019. Photocatalytic decomposition of N_2O over g-C_3N_4/$BiVO_4$ composite. Appl. Surf. Sci. 469, 181–191.
Richardson, J.T., Peng, Y., Remue, D., 2000. Properties of ceramic foam catalyst supports: pressure drop. Appl. Catal. A, 19–32.
Richardson, J.T., Remue, D., Hung, J.-K., 2003. Properties of ceramic foam catalyst supports: mass and heat transfer. Appl. Catal. A, 319–329.
Russo, N., 2007. N_2O catalytic decomposition over various spinel-type oxides. Catal. Today, 228–232.
Russo, N., Fino, D., Saracco, G., Specchia, V., 2007. N_2O catalytic decomposition over various spinel-type oxides. Catal. Today 119, 228–232.
Schatte, G., Shen, J., Reaney, M., Sammynaiken, R., 2011. Poly[μ-(1,3-dihy-droxy-propan-2-olato)-potassium]. Acta Crystallogr. Sect. E: Struct. Rep. Online, m141–m142.
Shi, L. et al., 2012. Studies on surface impregnation combustion method to prepare supported Co/SiO_2 catalysts and its application for Fisher-Tropsch synthesis. Appl. Catal. A, 217–224.
Specchia, S., Finocchio, E., Busca, G., Specchia, V. Combustion Synthesis, Handbook of Combustion, pp. 439-472.
Twigg, M.V., Richardson, J.T., 2002. Theory and applications of ceramic foam catalysts. Chem. Eng. Res. Des., 183–189.
Varma, A., Mukasyan, A.S., Rogachev, A.S., Manukyan, K.V., 2016. Solution combustion synthesis of nanoscale materials. Chem. Rev. 116, 14493–14586.
Wójcik, S., Grzybek, G., Gryboś, J., Kotarba, A., Sojka, Z., 2018. Designing, optimization and performance evaluation of the K-$Zn_{0.4}Co_{2.6}O_4$|α-Al_2O_3|cordierite catalyst for low-temperature N_2O decomposition. Catal. Commun. 110, 64–67.
Wójcik, S., Ercolino, G., Gajewska, M., Quintero, C.W.M., Specchia, S., Kotarba, A., 2018. Robust Co_3O_4|α-Al_2O_3|cordierite structured catalyst for N_2O abatement – validation of the SCS method for active phase synthesis and deposition. Chem. Eng. J. 377, 120088.
Wójcik, S., Grzybek, G., Stelmachowski, P., Sojka, Z., Kotarba, A., 2020. Bulk, surface and interface promotion of Co_3O_4 for the Low-temperature N_2O decomposition catalysis. Catalysts 10, 41.
Wulff, G., 1901. Zur Frage der Geschwindigkeit des Wachstums und der Auflösung der Krystallflagen. Z. Kristallogr. - Cryst. Mater. 34, 449–530.
Wyrwalski, F. et al., 2007. Modified Co_3O_4/ZrO_2 catalysts for VOC emissions abatement. Catal. Today, 332–337.
Yoshino, H., Ohnishi, C.H., Hosokawa, S., Wada, K., Inoue, M., 2011. Optimized synthesis method for K/Co_3O_4 catalyst towards direct decomposition of N_2O. J. Mater. Sci. 46, 797–805.
Zasada, F., Piskorz, W., Cristol, S., Paul, J.-F., Kotarba, A., Sojka, Z., 2010. Periodic density functional theory and atomistic thermodynamic studies of cobalt spinel nanocrystals in wet environment: molecular interpretation of water adsorption equilibria. J. Phys. Chem. C 114, 22245–22253.
Zasada, F., Pinho, P.V.B., Piskorz, W., Hudy, C., Janas, J., Grybo, K., Góra-Marek, Z.S., 2020. Adsorption of NO_2 and NO_3 on cobalt spinel nanocubes and interfacial dynamics of the resultant NOx adspecies (x = 1, 2, and 3): DFT, atomistic thermodynamic, IR, and isotopic exchange study. J. Phys. Chem. C 124, 19681–19697.
Zavyalova, U., Scholz, P., Ondruschka, B., 2007. Influence of cobalt precursor and fuels on the performance of combustion synthesized Co_3O_4/(g)-Al_2O_3 catalysts for total oxidation of methane. Appl. Catal. A: General, 226–233.
Zavyalova, U., Girgsdies, F., Korup, O., Horn, R., Schlögl, R., 2009. Microwave-assisted self-propagating combustion synthesis for uniform deposition of metal nanoparticles on ceramic monoliths. J. Phys. Chem. C 113, 17493–17501.